THE JOURNAL OF BIOLOGICAL CHEMISTRY
Vol. 274, No. 52, Issue of December 24, pp. 37060–37069, 1999

Printed in U.S.A.

Poliovirus RNA-dependent RNA Polymerase ($3D^{pol}$)

DIVALENT CATION MODULATION OF PRIMER, TEMPLATE, AND NUCLEOTIDE SELECTION*

(Received for publication, May 10, 1999, and in revised form, August 7, 1999)

Jamie J. Arnold, Saikat Kumar B. Ghosh, and Craig E. Cameron‡

From the Department of Biochemistry and Molecular Biology, Pennsylvania State University, University Park, Pennsylvania 16802

We have analyzed the divalent cation specificity of poliovirus RNA-dependent RNA polymerase, $3D^{pol}$. The following preference was observed: $Mn^{2+} > Co^{2+} > Ni^{2+} > Fe^{2+} > Mg^{2+} > Ca^{2+} > Cu^{2+}$, and Zn^{2+} was incapable of supporting $3D^{pol}$-catalyzed nucleotide incorporation. In the presence of Mn^{2+}, $3D^{pol}$ activity was increased by greater than 10-fold relative to that in the presence of Mg^{2+}. Steady-state kinetic analysis revealed that the increased activity observed in the presence of Mn^{2+} was due, primarily, to a reduction in the K_M value for $3D^{pol}$ binding to primer/template, without any significant effect on the K_M value for nucleotide. The ability of $3D^{pol}$ to catalyze RNA synthesis *de novo* was also stimulated approximately 10-fold by using Mn^{2+}, and the enzyme was now capable of also utilizing a DNA template for primer-independent RNA synthesis. Interestingly, the use of Mn^{2+} as divalent cation permitted $3D^{pol}$ activity to be monitored by following extension of 5′-^{32}P-end-labeled, heteropolymeric RNA primer/templates. The kinetics of primer extension were biphasic because of the enzyme binding to primer/template in both possible orientations. When bound in the incorrect orientation, $3D^{pol}$ was capable of efficient addition of nucleotides to the blunt-ended duplex; this activity was also apparent in the presence of Mg^{2+}. In the presence of Mn^{2+}, $3D^{pol}$ efficiently utilized dNTPs, ddNTPs, and incorrect NTPs. On average, three incorrect nucleotides could be incorporated by $3D^{pol}$. The ability of $3D^{pol}$ to incorporate the correct dNTP, but not the correct ddNTP, was also observed in the presence of Mg^{2+}. Taken together, these results provide the first glimpse into the nucleotide specificity and fidelity of the poliovirus polymerase and suggest novel alternatives for the design of primer/templates to study the mechanism of $3D^{pol}$-catalyzed nucleotide incorporation.

Positive-strand RNA viruses represent an existing and emerging threat to the United States public health. For example, as many as 4 million Americans are currently infected by hepatitis C virus. Hepatitis C virus is capable of establishing a persistent infection, which leads to cirrhosis of the liver and, in some cases, liver cancer (1). Unfortunately, highly effective therapies to treat chronic RNA virus infection do not exist. Replication of the genomes of all RNA viruses requires the virus-encoded RNA-dependent RNA polymerase (RdRP)[1] (2). RdRP activity is unique to virus-infected, human cells; therefore, the RdRP is a suitable target for the development of antiviral agents. Although RdRPs from several viruses have been purified and characterized to some extent, a large gap remains in terms of our understanding of the biochemical mechanism of this class of nucleic acid polymerase relative to those classes of polymerase involved in cellular processes such as replication and transcription (2–8). A detailed kinetic and thermodynamic description of RdRP-catalyzed nucleotide incorporation should permit this enzyme to be distinguished from cellular polymerases, thus facilitating the development of RdRP-specific inhibitors useful for the treatment of RNA virus infection.

Biological and biochemical studies of poliovirus genome replication have been ongoing for decades (9). These studies have shown that RNA structures at the 3′-end of the genome (10), and possibly at the 5′-end of the genome (11), specify the site of assembly of the replication complex. The exact composition and order of assembly of this complex remains to be determined. However, both viral and host factors have been implicated in replicase assembly and/or function (12–15). After complex assembly, poliovirus RNA-dependent RNA polymerase, $3D^{pol}$, initiates RNA synthesis by using the protein primer, 3B (VPg). $3D^{pol}$ has been studied intensively for many years because of its key role in poliovirus genome replication. Therefore, this enzyme is an ideal model system to use in the study of RdRP mechanism and for the elucidation of RdRP structure-function relationships.

In vitro studies employing pure, active $3D^{pol}$ have identified many of the biochemical properties and enzymatic activities associated with this enzyme. In addition to oligo(dT)- and oligo(rU)-dependent poly(rU) polymerase activity (3, 4), $3D^{pol}$ is capable of uridylylating VPg and utilizing the resulting VPg-pUpU product as a primer for poly(rU) synthesis (16). $3D^{pol}$ has terminal transferase activity (17) and strand displacement activity (18). Also, $3D^{pol}$ has the ability to multimerize (19), and Kirkegaard and colleagues (20) have suggested that multimerization may be required for nucleic acid binding, polymerase activity (21), and virus viability (22). Recently, we demonstrated that $3D^{pol}$ is sufficient for template switching, and this enzyme is capable of catalyzing primer-independent RNA synthesis (23). Finally, a high resolution crystal structure is available for $3D^{pol}$ (19). The overall topology of $3D^{pol}$ is quite similar to that of the other classes of nucleic acid polymerase in that the enzyme resembles a right hand with "fingers," "palm," and "thumb" subdomains. The palm subdomain contains four struc-

* This work was supported in part by Howard Temin Award CA75118 from the NCI, National Institutes of Health (to C. E. C.). The costs of publication of this article were defrayed in part by the payment of page charges. This article must therefore be hereby marked "*advertisement*" in accordance with 18 U.S.C. Section 1734 solely to indicate this fact.

‡ To whom correspondence should be addressed. Tel.: 814-863-8705; Fax: 814-863-7024; E-mail: cec9@psu.edu.

[1] The abbreviations used are: RdRP, RNA-dependent RNA polymerase; PAGE, polyacrlyamide gel electrophoresis; TLC, thin-layer chromatography; NTP, nucleoside-5′-triphosphate; dNTP, 2′-deoxynucleoside-5′-triphosphate; ddNTP, 2′,3′-dideoxynucleoside-5′-triphosphate; NMP, nucleoside-5′-monophosphate; dNMP, 2′-deoxynucleoside-5′-monophosphate; ddNMP, 2′,3′-dideoxynucleoside-5′-monophosphate; PP_i, pyrophosphate.

tural motifs (A–D) found in all polymerases, in addition to a fifth motif (E) found only in enzymes, such as reverse transcriptases, which utilize RNA templates.

Clearly, a great deal of information germane to 3D^{pol} function exists. However, detailed kinetic and mechanistic studies of this enzyme have yet to be performed. The absence of this information greatly limits the extent to which structural information can be exploited to establish the structure-function relationships of this class of polymerase. Detailed kinetic and mechanistic investigations of 3D^{pol} have been limited, primarily, by the inability to establish stoichiometric complexes between 3D^{pol} and primer/template that permit polymerase activity to be monitored by following the extension of end-labeled, heteropolymeric RNA primers. One possible explanation for this is that 3D^{pol} has a low affinity for nucleic acid. We have shown that the K_M value of 3D^{pol} for short, homopolymeric primer/templates is in the 10–20 μM range (23), and Kirkegaard and colleagues (20) have reported K_d values for 3D^{pol} binding to nucleic acid that are in the μM range.

In this report, we have extended our systematic, quantitative analysis of 3D^{pol} by evaluating the divalent cation specificity of this enzyme. Taken together, the data described herein provide evidence for functional similarity between the RdRP and DNA polymerases and suggest novel strategies for the design of primer/template substrates to investigate 3D^{pol} mechanism.

EXPERIMENTAL PROCEDURES

Materials

[α-^{32}P]GTP (>3,000 Ci/mmol), [α-^{32}P]UTP (>6,000 Ci/mmol), and [γ-^{32}P]GTP (>6,000 Ci/mmol) were from NEN Life Science Products; [γ-^{32}P]ATP (>7,000 Ci/mmol) was from ICN; nucleoside 5′-triphosphates, 2′-deoxynucleoside 5′-triphosphates, 2′,3′-deoxynucleoside 5′-triphosphates (all nucleotides were ultrapure solutions), and poly(rA) were from Amersham Pharmacia Biotech, Inc.; poly(rC) and poly(U) were from Sigma; all DNA oligonucleotides were from Operon Technologies, Inc. (Alameda, CA); all RNA oligonucleotides were from Dharmacon Research, Inc. (Boulder, CO); 10-base pair DNA ladder was from Life Technologies, Inc.; T4 polynucleotide kinase and calf intestinal alkaline phosphatase were from New England Biolabs, Inc.; $MgCl_2$, $MnCl_2$, $ZnCl_2$, and $CaCl_2$ were from Fisher; $CuCl_2$, $FeCl_2$, $NiCl_2$, $CoCl_2$, and GpG were from Sigma; polyethyleneimine-cellulose TLC plates were from EM Science; 2.5-cm DE81 filter paper discs were from Whatman. All other reagents were of the highest grade available from Sigma or Fisher.

Expression and Purification of 3D^{pol}

Expression and purification of 3D^{pol} was performed as described previously (23, 24).

Purification of Synthetic Oligonucleotides

DNA and RNA oligonucleotides were purified by denaturing PAGE. Gels consisted of: 19% acrylamide, 1% bisacrylamide, 7 M urea and 1 × TBE (89 mM Tris base, 89 mM boric acid, and 2 mM EDTA). The oligonucleotide ladder was visualized by UV shadowing. A gel slice containing only the full-length oligonucleotide was removed, and the nucleic acid was electroeluted from the gel in 1 × TBE by using an Elutrap apparatus (Schleicher & Schuell). Oligonucleotides were desalted on Sep-Pak columns (Millipore) as specified by the manufacturer. Oligonucleotides were typically suspended in $T_{10}E_1$ (10 mM Tris, 1 mM EDTA, pH 8.0), aliquoted, and stored at −80 °C until use. Concentrations were determined by measuring the absorbance at 260 nm by using calculated extinction coefficients (25).

Purity of [α-^{32}P]NTPs

[α-^{32}P]NTPs were diluted to 0.1 μCi/μl in ddH_2O, and 1 μl was spotted in triplicate onto TLC plates. TLC plates were developed in 0.3 M potassium phosphate, pH 7.0, dried, and exposed to a PhosphorImager screen. Imaging and quantitation were performed by using the ImageQuant software from Molecular Dynamics. The purity was used to correct the specific activity of NTP in reactions to calculate accurate concentrations of product. Purity was checked before or after each experiment and ranged from 50 to 90%.

5′-^{32}P Labeling of Oligonucleotides

DNA and RNA oligonucleotides were end-labeled by using [γ-^{32}P]ATP and T4 polynucleotide kinase essentially as specified by the manufacturer. Reactions typically contained 11 μM [γ-^{32}P]ATP, 10 μM DNA, or RNA oligonucleotide, and 0.4 unit/μl T4 polynucleotide kinase. Unincorporated nucleotide was removed by passing the sample over two consecutive 1-ml Sephadex G-25 (Sigma) spun columns.

5′-^{32}P Labeling of DNA Ladder

Labeling of the DNA ladder was performed by using [γ-^{32}P]ATP and T4 polynucleotide kinase as specified by Life Technologies, Inc.

5′-^{32}P Labeling of GpG

GpG was end-labeled by using [γ-^{32}P]ATP and T4 polynucleotide kinase essentially as specified by the manufacturer. Reactions typically contained 1 μM [γ-^{32}P]ATP, 10 μM GpG, and 0.4 unit/μl T4 polynucleotide kinase. Reactions were quenched by heating the reaction at 60 °C for 5 min.

Annealing of Heteropolymeric Primer/Templates

1 μM end-labeled RNA primer was mixed with 9 μM unlabeled RNA primer and 10 μM unlabeled RNA template in $T_{10}E_1$ and heated to 90 °C for 1 min and slowly cooled to 10 °C at a rate of approximately 5 °C/min in a Progene thermocycler.

3D^{pol} Assays

Reactions contained 50 mM HEPES, pH 7.5, 10 mM 2-mercaptoethanol, 5 mM $MgCl_2$ or $MnCl_2$, 60 μM $ZnCl_2$, 500 μM NTP, primer/template and 3D^{pol}. Reactions were quenched by the addition of EDTA to a final concentration of 50 mM. Specific concentrations of primer/template and 3D^{pol}, along with any deviations from the above, are indicated below or in the appropriate figure legend.

Divalent Cation Modulation of 3D^{pol} Poly(rU) and Poly(rG) Polymerase Activity

Reactions contained 0.5 μM 3D^{pol}, 500 μM nucleotide (UTP or GTP), 0.2 μCi/μl radiolabeled nucleotide ([α-^{32}P]UTP or [α-^{32}P]GTP), either $MgCl_2$ or $MnCl_2$ (5 mM) and either dT_{15} (1.88 μM) and poly(rA) (93.4 μM AMP), or dG_{15} (1.88 μM) and poly(rC) (93.4 μM CMP), or dT_{15}/rA_{30} (1 μM) or dG_{15}/rC_{30} (1 μM). Reactions were initiated by the addition of 3D^{pol} and incubated at 30 °C for 5 min. Reaction volumes were 25 μl.

Optimal Divalent Cation Concentration for Maximal Activity

Reactions contained 3D^{pol} (0.1 μM), dG_6 (4.7 μM), poly(rC) (93.4 μM CMP), GTP (500 μM), [α-^{32}P]GTP (0.2 μCi/μl, 0.07 μM) and either $MgCl_2$ or $MnCl_2$. Reactions were initiated by addition of 3D^{pol} and incubated at 30 °C for 5 min at which time the reactions were quenched by addition of EDTA to a final concentration of 50 mM. Reaction volumes were 25 μl. Products were analyzed by DE81 filter binding.

RNA Synthesis de Novo: Template Specificity

Reactions contained 3D^{pol} (0.5 μM), GTP (500 μM), [α-^{32}P]GTP (0.2 μCi/μl, 0.07 μM), either $MgCl_2$ (5 mM) or $MnCl_2$ (5 mM) and either rC_{30} (10 μM), dC_{30} (10 μM), or poly(rC) (300 μM CMP). Reactions were initiated by addition of 3D^{pol} and incubated at 30 °C for 10 min. Reaction volumes were 50 μl. Products were analyzed by DE81 filter binding.

Steady-state Kinetic Analysis of 3D^{pol}

Kinetic constants, K_M and V_{max}, were determined by using the assay described above. The concentration of 3D^{pol} employed in these experiments ranged from 0.01 to 0.5 μM depending upon the substrate and cation employed. The V_{max} values reported in Table III have been normalized to 0.01 μM 3D^{pol} to facilitate comparison of the various substrates. Concentrations of the varied substrate, nucleic acid or nucleotide, ranged from 0.25 × K_M to 4 × K_M. The concentration of the substrate that remained constant was 5–10 × K_M. Single time points were taken that were in the linear range for product formation. Reaction rates were plotted as a function of substrate concentration, and these data were fit to a hyperbola by nonlinear regression using the program KaleidaGraph (Synergy Software, Reading, PA) to obtain the kinetic constants. In one instance, the determination of the K_M value for GTP in the presence of $MgCl_2$, the enzyme was not saturated with dG_{15}/rC_{30} primer/template, thus the K_M(app) is reported. However, the true K_M was calculated by using Equation 1.

TABLE I
Divalent cation modulation of 3D^{pol} poly(rU) and poly(rG) polymerase activity

Reactions were performed as described under "Experimental Procedures." Activity values are reported using one significant figure, and the S.E. of the data was less than 10%.

Substrate	Activity	
	Mg^{2+}	Mn^{2+}
	pmol / min / μg	
dT_{15}/poly(rA)	1,000	10
dT_{15}/rA_{30}	10	100
dG_{15}/poly(rC)	200	1,000
dG_{15}/rC_{30}	2	200

$$K_M(\text{app})_{GTP} = K_{M,GTP}\left(1 + \frac{K_{M,dG_{15}/rC_{30}}}{[dG_{15}/rC_{30}]}\right) \quad \text{(Eq. 1)}$$

Divalent Cation Specificity of 3D^{pol}

Reactions contained 3D^{pol} (0.5 μM), dT_{15}/rA_{30} (1 μM), UTP (500 μM), [α-^{32}P]UTP (0.2 μCi/μl, 0.034 μM), and XCl_2 (5 mM), where $X = Zn^{2+}$, Cu^{2+}, Ca^{2+}, Mg^{2+}, Fe^{2+}, Ni^{2+}, Co^{2+}, and Mn^{2+}. Reactions were initiated by addition of 3D^{pol} and incubated at 30 °C for 10 min. Reaction volumes were 25 μl. In all cases, 5 mM was the optimal concentration for maximal activity. Products were analyzed by DE81 filter binding.

Phosphatase Treatment of [α-^{32}P]GTP- and [γ-^{32}P]GTP-labeled RNA Products

Phosphatase reactions were performed by using calf intestinal alkaline phosphatase and either [α-^{32}P]GTP- or [γ-^{32}P]GTP-labeled RNA essentially as described by the manufacturer. Reactions contained 0.1 unit/μl calf intestinal alkaline phosphatase and either [α-^{32}P]GTP-labeled RNA (300,000 cpm, 15 pmol) or [γ-^{32}P]GTP-labeled RNA (300,000 cpm, 100 pmol). Reaction volumes were 50 μl. Reactions were initiated by addition of calf intestinal alkaline phosphatase and incubated at 37 °C. Reactions were quenched by addition of EDTA to a final concentration of 50 mM. [α-^{32}P]GTP- and [γ-^{32}P]GTP-labeled RNA were prepared as follows: reactions contained 3D^{pol} (5 μM), rC_{30} (10 μM), GTP (500 μM), $MnCl_2$ (5 mM), and either [α-^{32}P]GTP (1 μCi/μl, 0.33 μM) or [γ-^{32}P]GTP (4 μCi/μl, 0.68 μM). Reactions were initiated by addition of 3D^{pol} and incubated at 30 °C for 5 min at which time reactions were quenched by addition of EDTA to a final concentration of 50 mM. Each quenched reaction was passed over two consecutive 1-ml Sephadex G-25 spun columns to remove any unincorporated nucleotide.

Product Analysis

DE81 Filter Binding—10 μl of the quenched reaction was spotted onto DE81 filter paper discs and dried completely. The discs were washed three times for 10 min in 250 ml of 5% dibasic sodium phosphate and rinsed in absolute ethanol. Bound radioactivity was quantitated by liquid scintillation counting in 5 ml of Ecoscint scintillation fluid (National Diagnostics).

TLC—1 μl of the quenched reaction was spotted onto TLC plates. TLC plates were developed in 0.3 M potassium phosphate, pH 7.0, dried, and exposed to a PhosphorImager screen.

Denaturing PAGE—Sample preparation and electrophoresis were as described previously (26). Briefly, 1 μl of the quenched reaction was added to 9 μl of loading buffer: 90% formamide, 50 mM Tris borate, 0.025% bromphenol blue, 0.025% xylene cyanol and where appropriate a 10-fold excess of unlabeled RNA (trap strand) relative to the end-labeled RNA under investigation was added. Samples were heated to 70 °C for 2–5 min prior to loading 5 μl on a 1× TBE, 7 M urea polyacrylamide gel of the appropriate percentage. Highly cross-linked gels contained 2% bisacrylamide. Electrophoresis was performed in 1 × TBE at 75 watts. Gels were visualized and quantitated by using a PhosphorImager.

RESULTS

Transition Metals Support 3D^{pol}-catalyzed Nucleotide Incorporation—We determined the effect of Mn^{2+} on 3D^{pol}-catalyzed nucleotide incorporation with the following substrates: dT_{15}/poly(rA), dT_{15}/rA_{30}, dG_{15}/poly(rC), and dG_{15}/rC_{30} (Table I). The stimulation of 3D^{pol} activity observed by using Mn^{2+} was substrate-dependent and varied from 5- to 100-fold the activity determined in the presence of Mg^{2+} (Table I). The 10-fold decrease in activity with dT_{15}/poly(rA) was due, most likely, to a decrease in the solubility in the presence of Mn^{2+} as a white precipitate could be observed after centrifugation of this reaction mixture. The precipitate formed in the presence or absence of enzyme. This phenomenon was not observed with other primer/template substrates.

TABLE II
Optimal divalent cation concentration for maximal activity and RNA synthesis de novo: template specificity

Reactions were performed as described under "Experimental Procedures."

	GMP incorporated	
	Mg^{2+}	Mn^{2+}
	pmol	
Concentration		
0.5 mM	55	172
1 mM	386	2,058
2.5 mM	691	2,356
5 mM	826	2,384
10 mM	759	2,162
50 mM	0	590
Substrate		
rC_{30}	17	2,250
dC_{30}	1	1,100
Poly(rC)	700	9,900

The optimal concentration for maximal 3D^{pol} activity was 5 mM (Table II). Concentrations of divalent cation greater than 10 mM were inhibitory (Table II). The observed inhibition did not appear to be due to precipitation of nucleic acid and/or enzyme. The K_M value for primer/template substrates was reduced by an average of 25-fold in the presence of Mn^{2+} relative to the corresponding values measured in the presence of Mg^{2+} (Table III). A 3-fold reduction in V_{max} was observed for dT_{15}/rA_{30} by using Mn^{2+} instead of Mg^{2+}; however, a 30-fold increase in V_{max} was observed for dG_{15}/rC_{30} by using Mn^{2+} instead of Mg^{2+}. The K_M values for UTP and GTP with the corresponding primer/template substrates were similar, 62 and 116 μM, respectively, and the V_{max} values were as expected based on the kinetic analysis of primer/template substrates discussed above. The increase in V_{max} observed in the presence of Mn^{2+} when dG_{15}/rC_{30} was employed did not result from a change in K_M value for GTP (Table III). Thus, an increase in the number of productive 3D^{pol}-dG_{15}/rC_{30} complexes formed may occur by using Mn^{2+} instead of Mg^{2+}. Mn^{2+}, Co^{2+}, Ni^{2+}, and Fe^{2+} supported higher levels of activity than Mg^{2+} (Table IV). Ca^{2+} and Cu^{2+} supported lower levels of activity than Mg^{2+} (Table IV). Zn^{2+} was incapable of supporting activity (Table IV).

Mn^{2+} Increases the Efficiency of 3D^{pol}-catalyzed RNA Synthesis de Novo—Recently, we reported that 3D^{pol} initiates RNA synthesis when poly(rC) and GTP are employed as the sole substrates (23). Primer-independent RNA synthesis did not result from a polynucleotide-phosphorylase-like activity as template was required (data not shown). Poly(rC) and GTP appear to be the most efficient substrates for this reaction as neither poly(rA) and UTP nor poly(rU) and ATP could be used to demonstrate convincingly synthesis of RNA (data not shown). In addition, rC_{30}, but not dC_{30}, was also a template for primer-independent RNA synthesis, albeit at a level 30-fold lower than observed by using poly(rC) (Table II). As shown in Table II, Mn^{2+} stimulated primer-independent RNA synthesis by 15-fold relative to reactions performed in the presence of Mg^{2+} when either poly(rC) or rC_{30} was employed as template. In the presence of Mn^{2+}, dC_{30} was also utilized as a template (Table II) and utilization of the dC_{30} template by 3D^{pol} was now only 2-fold less efficient than utilization of the rC_{30} template. Products of this reaction resolved by denaturing PAGE and

TABLE III
Steady-state kinetic analysis of 3D^{pol}
Steady-state kinetic analysis was performed as described under "Experimental Procedures."

Substrate varied	Cofactor	K_m	V_{max}	V_{max}/K_m
		μM	$\mu M/min$	$\times 10^{-3}$
Nucleic acid				
dT_{15}/rA_{30}[a]	$MgCl_2$	24.6 ± 2.8	0.182 ± 0.008	7.40
dT_{15}/rA_{30}	$MnCl_2$	0.88 ± 0.08	0.064 ± 0.002	73
dG_{15}/rC_{30}	$MgCl_2$	13.2 ± 3.9	0.005 ± 0.001	0.38
dG_{15}/rC_{30}	$MnCl_2$	0.75 ± 0.25	0.148 ± 0.014	197
rC_{30}	$MnCl_2$	0.034 ± .004	0.028 ± 0.008	824
Nucleotide				
UTP	$MnCl_2$	61.9 ± 9.5	0.044 ± 0.002	0.71
GTP	$MgCl_2$	158.3 ± 32.2[b]	0.010 ± 0.001	0.063
GTP(dG_{15}/rC_{30})	$MnCl_2$	116.1 ± 8.4	0.168 ± 0.006	1.45
GTP(rC_{30})	$MnCl_2$	92.9 ± 5.1	0.034 ± 0.001	0.34

[a] Taken from Arnold and Cameron (23).
[b] This value was not determined under saturating conditions of dG_{15}/rC_{30} and is therefore an apparent K_M value. The calculated K_M value is 80 μM (see "Experimental Procedures").

TABLE IV
Divalent cation specificity of 3D^{pol}
Reactions were performed as described under "Experimental Procedures."

Divalent cation	UMP incorporated
	pmol
Zn^{2+}	0
Cu^{2+}	3
Ca^{2+}	4
Mg^{2+}	9
Fe^{2+}	31
Ni^{2+}	38
Co^{2+}	97
Mn^{2+}	275

visualized by phosphorimaging were greater than unit length and similar in appearance to those produced via template switching when dG_{15}/rC_{30} and GTP are employed as substrates (23).

What is the mechanism of initiation of these long RNA products? One possibility is that the terminal transferase activity of 3D^{pol} adds GMP to the 3′-end of rC_{30}, thus creating a "snapback" substrate that is efficiently extended by 3D^{pol}. However, by using a 5′-end-labeled rC_{30} template, we were only able to show the incorporation of a single GMP into rC_{30} (data not shown). Moreover, the kinetics of formation of this product were too slow to support the hypothesis that $rC_{30}G$ RNA was the substrate used by 3D^{pol} to produce long products (data not shown). A second possibility is that RNA synthesis is initiated *de novo*. To test this possibility, we performed an experiment employing rC_{30} and [γ-^{32}P]GTP as substrates. If RNA synthesis initiates *de novo*, then long RNA products should incorporate the label. Product RNA was labeled by using [γ-^{32}P]GTP, thus long products most likely result from *de novo* initiation (Fig. 1*B*). The primary product of this reaction was the dinucleotide, pppGpG. Also, tri-, tetra-, and pentanucleotide products were observed. The dinucleotide product was assigned based upon the comigration of this product with ^{32}pGpG on polyacrylamide gels (data not shown). To keep a complete inventory of all products formed during the course of the reaction when [γ-^{32}P]GTP was employed, reaction mixtures were also resolved by TLC; over half of the nucleotide was utilized based on PP_i accumulation (Fig. 1*C*). Phosphatase treatment of [γ-^{32}P]GTP-labeled RNA showed a time-dependent loss of label by using the DE81 filter paper method (Fig. 2*A*) and PAGE (Fig. 2*B*) without any change in label associated with the control, [α-^{32}P]GTP-labeled RNA (Fig. 2, *A* and *B*). Greater than 95% of the counts associated with [γ-^{32}P]GTP-labeled RNA originated from [γ-^{32}P]GTP, thus confirming that this RNA was initiated *de novo*.

Quantitative analysis of the kinetics of product formation in reactions employing either [γ-^{32}P]GTP or [α-^{32}P]GTP as substrates showed that both reactions displayed burst kinetics (Fig. 3*A*). In both cases, the steady-state rates (linear phases) of product formation were identical; however, the burst amplitude of PP_i formation measured by TLC was 5-fold greater than that of RNA measured by using the DE81 filter binding method. This difference likely reflects the inability of DE81 filter paper to retain dinucleotide product. Although the burst of PP_i formation cannot be used directly to quantitate active sites, the burst can be exploited to compare the "active" fraction of various enzyme preparations.

In contrast, quantitation of the kinetics of [γ-^{32}P]GTP-labeled RNA formation should report directly on the concentration of active sites if a burst of product formation is observed. When this analysis was performed, an apparent burst of labeled RNA was observed (Fig. 3*B*). However, based on the concentration of enzyme employed, the burst amplitude was 6–7-fold greater than the enzyme concentration. Because the enzyme concentration was determined by measuring the protein absorbance at 280 nm under denaturing conditions and using a calculated extinction coefficient of 71,830 M^{-1} cm^{-1} (24, 27, 28), it is unlikely that the enzyme concentration was grossly underestimated. The most reasonable explanation for this observation is that multiple rounds of abortive initiation events occur producing dinucleotide product prior to synthesis of completely elongated RNA.

Steady-state kinetic analysis of this reaction in the presence of Mn^{2+} showed that the catalytic efficiency of this reaction is greater than either of the primer-dependent reactions characterized (Table III). The K_M value of 3D^{pol} for GTP in the *de novo* reaction was virtually identical to that measured for GTP in the primer-dependent reaction (Table III). The ability to saturate the enzyme with reasonably low levels of template RNA coupled with the high catalytic efficiency could be useful for the rapid characterization of the nucleic acid binding properties of 3D^{pol} by evaluating the ability of "competitor" nucleic acids to inhibit RNA synthesis *de novo*.

Mn^{2+} Stimulates 3D^{pol}-catalyzed Extension of Heteropolymeric RNA Primer/Templates—The observation that the number of productive 3D^{pol}-dG_{15}/rC_{30} complexes that formed was increased by using Mn^{2+} instead of Mg^{2+} suggested that an increase in the utilization of heteropolymeric RNA primer/templates might also be observed by using Mn^{2+}. Two different primer/template substrates were employed (see Fig. 4, *A* and *D*). Both substrates consist of a 15-nucleotide primer and a 21-nucleotide template, which when annealed form a primer/

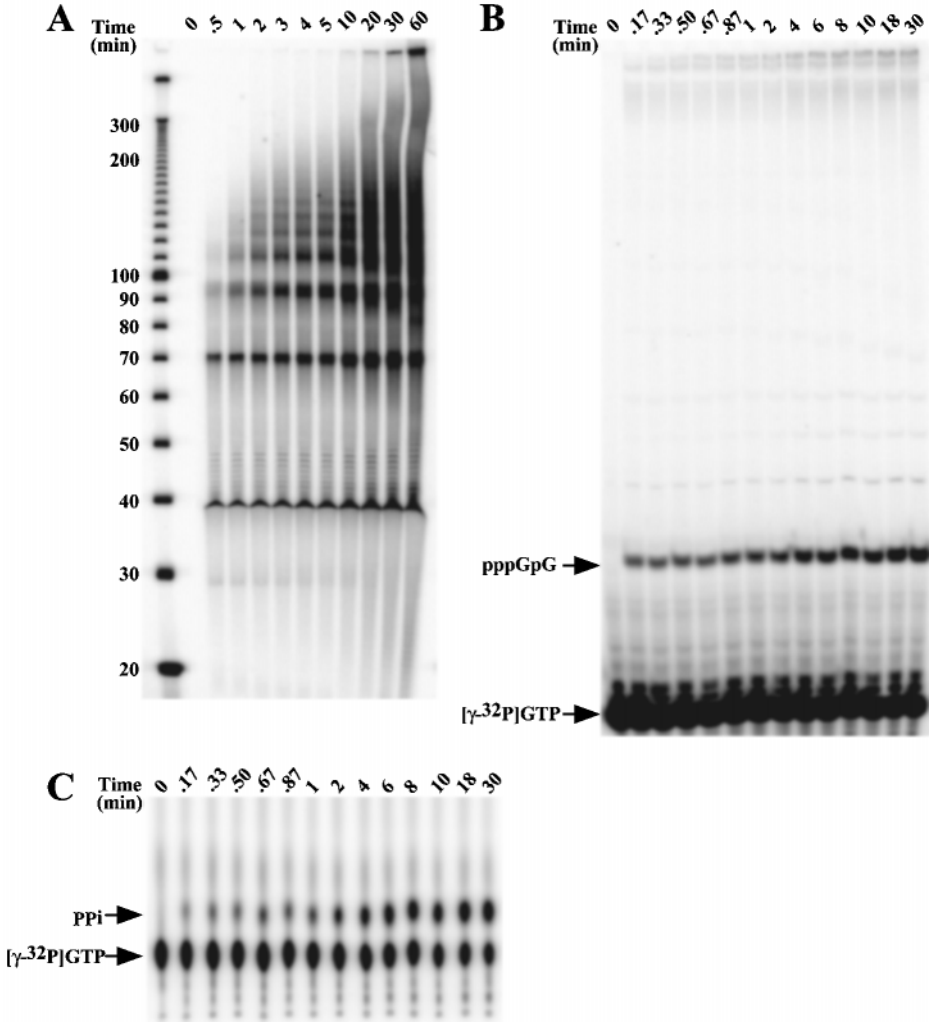

FIG. 1. **RNA synthesis *de novo*: product analysis.** *A*, reactions contained 3D^{pol} (1 μM), rC_{30} (10 μM), GTP (500 μM), [α-^{32}P]GTP (0.5 μCi/μl, 0.17 μM), and $MnCl_2$ (5 mM). Reactions were initiated by addition of 3D^{pol} and incubated at 30 °C; reactions were quenched at the indicated times by addition of EDTA to a final concentration of 50 mM. Products were resolved by electrophoresis on a denaturing 8% polyacrylamide gel. The size of selected bands from the single-stranded DNA ladder is indicated as a reference. *B*, reactions contained 3D^{pol} (1 μM), rC_{30} (10 μM), GTP (500 μM), [γ-^{32}P]GTP (2 μCi/μl, 0.34 μM), and $MnCl_2$ (5 mM). Reactions were initiated by addition of 3D^{pol} and incubated at 30 °C; reactions were quenched at the indicated times by addition of EDTA to a final concentration of 50 mM. Products were resolved by electrophoresis on a highly cross-linked, denaturing 23% polyacrylamide gel. *C*, reactions contained 3D^{pol} (1 μM), rC_{30} (10 μM), GTP (500 μM), [γ-^{32}P]GTP (2 μCi/μl, 0.34 μM), and $MnCl_2$ (5 mM). Reactions were initiated by addition of 3D^{pol} and incubated at 30 °C; reactions were quenched at the indicated times by addition of EDTA to a final concentration of 50 mM. Products were resolved by TLC.

template substrate containing a 15-base pair duplex and a 6-nucleotide, single-stranded 5′-overhang. These primer/templates differ from each other in two significant ways. First, the calculated T_M values are different (29). Primer/template I has a calculated T_M value of ~ 70 °C; primer/template II has a calculated T_M value of ~80 °C. Second, by using primer/template I and UTP, multiple cycles of correct nucleotide incorporation should occur; whereas by using primer/template II and ATP, only a single cycle of correct nucleotide incorporation should occur.

With primer/template I, where multiple cycles of nucleotide incorporation should occur by using UTP as the sole nucleotide substrate, primer was extended to the end of template (Fig. 4*B*). Once the primer was extended to the end of template, however, additional nucleotides (~20) were added, most likely a result of slippage synthesis. Products consistent with template switching were not observed. With primer/template II, where a single round of nucleotide incorporation should occur by using ATP as the sole nucleotide substrate, the first nucleotide was incorporated and misincorporation was noted (Fig. 4*E*). However, with each round of misincorporation, subsequent cycles of misincorporation became less efficient as very few primers could be extended to the end of template.

In both cases, the kinetics of primer extension were biphasic (Fig. 4,*C* and *F*). The first phase was faster than could be measured by manual quenching of the reaction. When primer/template I was employed, the amplitude of the first phase represented 65% of this substrate. When primer/template II was employed, the amplitude of the first phase represented 30% of this substrate. Whereas 85% of primer/template I was utilized during the course of the reaction, only 70% of primer/template II was utilized. When the kinetics of primer extension in the presence of Mn^{2+} from primer/template II were compared with the kinetics in the presence of Mg^{2+}, the primary difference observed was that more complexes formed in the presence of Mn^{2+} than in the presence of Mg^{2+}, both productive (note difference in *y* intercept in Fig. 5*A*) and nonproductive (note difference in end points in Fig. 5*A*). This conclusion was the same whether the first correct nucleotide (Fig. 5*A*) or all four nucleotides (Fig. 5*B*) were provided. However, it should be noted that the use of all four nucleotides supported higher levels of primer extension in the presence of both Mg^{2+} and Mn^{2+} than the use of a single nucleotide.

3D^{pol} Adds Nontemplated Nucleotides to Blunt-ended, Heteropolymeric RNA Primer/Templates—We reasoned that the biphasic nature of the kinetics was a reflection of enzyme binding in the "correct" orientation in some cases (fast incorporation) and in the "incorrect" orientation in others (slower incorporation). We performed experiments with primer/templates I and II in which the template strand was end-labeled instead of the primer strand (Fig. 6, *A* and *C*). Nontemplated addition of nucleotides was observed with both primer/templates in the presence of either Mn^{2+} or Mg^{2+} (Fig. 6, *B* and *D*). The reaction was more efficient in the presence of Mn^{2+} than in the presence of Mg^{2+}. Consistent with the amplitudes observed when labeled primers were employed, the template strand of primer/template I was utilized by 3D^{pol} with a lower efficiency than the template strand of primer/template II.

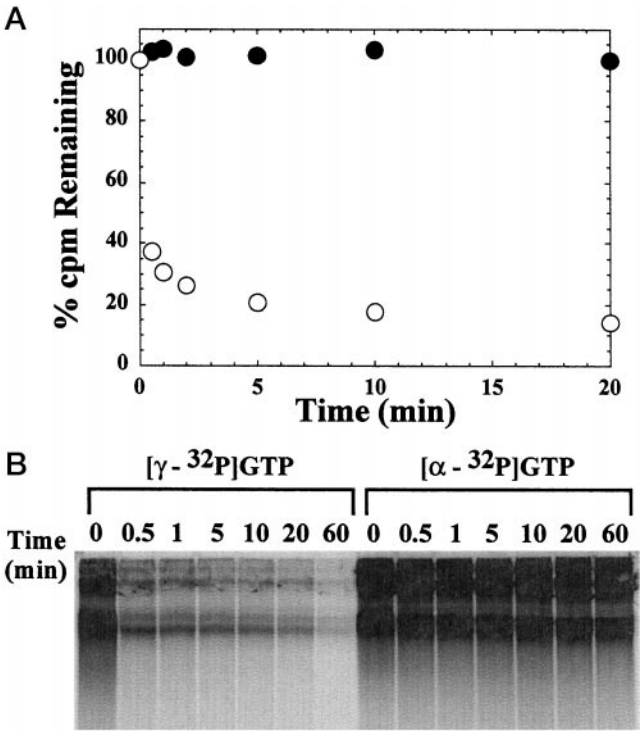

FIG. 2. **RNA synthesis *de novo*: phosphatase sensitivity of [γ-^{32}P]GTP-labeled RNA products.** [α-^{32}P]GTP- and [γ-^{32}P]GTP-labeled RNA were prepared as described under "Experimental Procedures." Reactions contained calf intestinal alkaline phosphatase (0.1 unit/μl) and either [α-^{32}P]GTP-labeled RNA (300,000 cpm, 15 pmol) or [γ-^{32}P]GTP-labeled RNA (300,000 cpm, 100 pmol). Reaction volumes were 50 μl. Reactions were initiated by addition of calf intestinal alkaline phosphatase and incubated at 37 °C. Reactions were quenched at the indicated times by addition of EDTA to a final concentration of 50 mM. *A*, products were analyzed by DE81 filter binding: ●, [α-^{32}P]GTP-labeled RNA; ○, [γ-^{32}P]GTP-labeled RNA. *B*, products were resolved by electrophoresis on a highly cross-linked, denaturing 23% polyacrylamide gel.

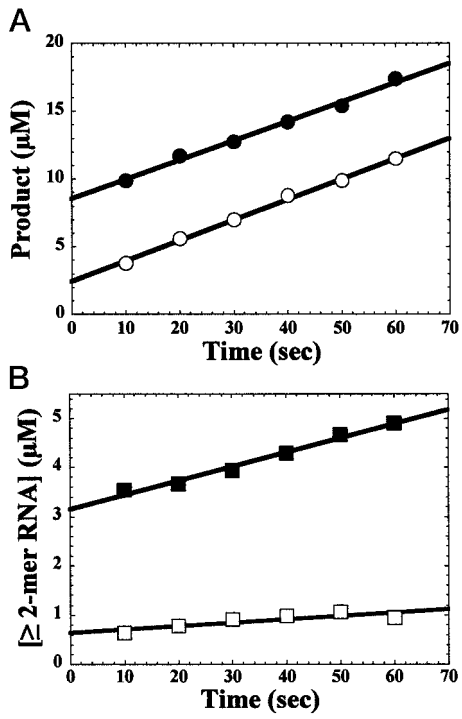

FIG. 3. **RNA synthesis *de novo*: kinetics of PP$_i$ production, GMP incorporation, and RNA production.** *A*, reactions contained 3D^{pol} (1 μM), rC$_{30}$ (10 μM), GTP (500 μM), $MnCl_2$ (5 mM), and either [γ-^{32}P]GTP (2 μCi/μl, 0.34 μM) or [α-^{32}P]GTP (0.5 μCi/μl, 0.17 μM). Reactions were initiated by addition of 3D^{pol} and incubated at 30 °C; reactions were quenched at the indicated times by addition of EDTA to a final concentration of 50 mM. Products were analyzed by either TLC or DE81 filter binding to determine the kinetics of PP$_i$ production (●) or GMP incorporation (○), respectively. *B*, kinetics of RNA production from reactions containing rC$_{30}$ (10 μM), GTP (500 μM), [γ-^{32}P]GTP (1 μCi/μl, 0.17 μM), $MnCl_2$ (5 mM), and either 0.5 μM (■) or 0.1 μM (□) 3D^{pol}. Reactions were initiated by addition of 3D^{pol} and incubated at 30 °C; reactions were quenched at the indicated times by addition of EDTA to a final concentration of 50 mM. Products were resolved by electrophoresis on a highly cross-linked, denaturing 23% polyacrylamide gel, visualized by using a PhosphorImager and quantitated by using the ImageQuant software (Molecular Dynamics).

The ability of 3D^{pol} to add nontemplated nucleotides to the blunt end of an RNA primer/template was somewhat surprising. However, it has been reported previously that the reverse transcriptase from human immunodeficiency virus has a similar activity (30). Terminal transferase activity of 3D^{pol} would yield similar results if single-stranded RNA were present in the reactions described above. We performed an experiment in which either the end-labeled primer (Fig. 7*A*) or template (Fig. 7*C*) strand of primer/template II was incubated with 3D^{pol}, ATP, and either Mg^{2+} or Mn^{2+} as the divalent cation. In all cases, the kinetics and/or products of the terminal transferase reaction were substantially different from those observed by using a template-labeled primer/template (Fig. 7, *B* and *D*). The ability of 3D^{pol} to partition in both possible orientations on heteropolymeric RNA primer/templates must be considered in any quantitative analysis of 3D^{pol}-catalyzed RNA synthesis.

3D^{pol} Is an RdRP and a Reverse Transcriptase—The ability to monitor 3D^{pol} activity by primer extension permitted us to evaluate the specificity and fidelity of 3D^{pol}-catalyzed nucleotide incorporation. In the presence of Mg^{2+}, both the correct rNMP and dNMP were incorporated to the greatest extent (Fig. 8*B*). With the correct rNTP, 40% of primers were extended (Fig. 8*B*, *lane 4*). In most cases, primers were extended to the end of template and additional nucleotides were added. The addition of extra nucleotides was most likely the result of slippage synthesis. However, it is also plausible that the extra nucleotides were added in a nontemplated fashion as discussed above. With the correct dNTP, 30% of primers were extended (Fig. 8*B*, *lane 8*). Whereas some primers were extended to the end of template, products with only a single dNMP incorporated accumulated to the greatest extent. Products greater than unit length were not observed. In the presence of Mg^{2+}, the correct ddNMP was not incorporated at all. The $n + 1$ product observed in *lane 12* of Fig. 8*B* must arise from rNTP contamination of the ddNTP stock. This conclusion is based on the migration of this product through the polyacrylamide gel; the $n + 1$ product present in *lane 12* of Fig. 8*B* is migrating slower than expected for a ddNMP-incorporated product (*cf.* Fig. 8*B*, *lane 12*, and Fig. 8*C*, *lane 26*).

In the presence of Mn^{2+}, a 2-fold increase in primer utilization was observed when either the correct rNTP (Fig. 8*C*, *lane 18*) or the correct dNTP (Fig. 8*C*, *lane 22*) was employed. 84% of primers were extended when the correct rNTP was utilized; and 72% of primers were extended when the correct dNTP was utilized. Interestingly, by using Mn^{2+} as the divalent cation, the correct ddNTP was utilized, and 34% of primers were extended (Fig. 8*C*, *lane 26*). The efficiency of correct rNMP and dNMP incorporation was also stimulated by using Mn^{2+}. In both cases, 90% of extended primers reached the end of template and addition of extra nucleotides was enhanced significantly (*cf.* Fig. 8*B*, *lanes 4* and *8*, and Fig. 8*C*, *lanes 18* and *22*).

Mn^{2+} Decreases the Fidelity of 3D^{pol}-catalyzed Nucleotide Incorporation—In the presence of Mg^{2+}, the efficiency of utilization of incorrect rNTPs (Fig. 8*B*, *lanes 1–3*), dNTPs (Fig. 8*B*, *lanes 5–7*), and ddNTPs (Fig. 8*B*, *lanes 9–11*) was less than 20%

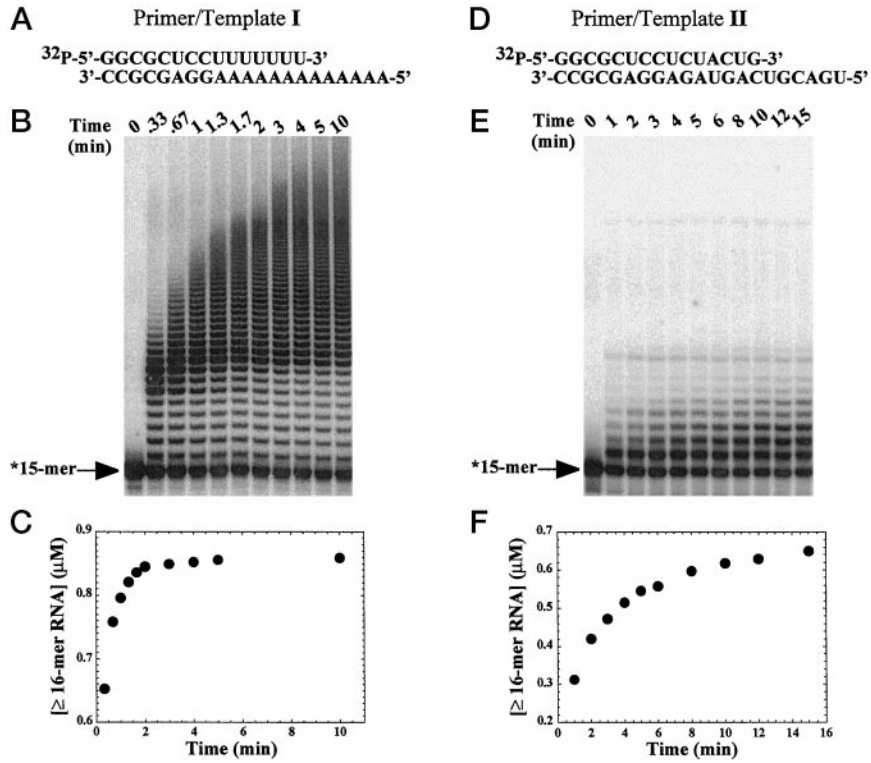

FIG. 4. **Primer Extension by 3D^{pol} in $MnCl_2$.** *A*, 15/21-mer primer/template I employed in the experiment described in *B*. *B*, reactions contained 3D^{pol} (5 μM), end-labeled primer/template I (1 μM), UTP (500 μM), and $MnCl_2$ (5 mM). Reactions were initiated by addition of 3D^{pol} and incubated at 30 °C; reactions were quenched at the indicated times by addition of EDTA to a final concentration of 50 mM. Products were resolved by electrophoresis on a denaturing 20% polyacrylamide gel. *C*, kinetics of primer extension in the reaction described in *B* were determined by quantitating product by using the ImageQuant software. *D*, 15/21-mer primer/template II employed in the experiment described in *E*. *E*, reactions contained 3D^{pol} (5 μM), end-labeled primer/template II (1 μM), ATP (500 μM), and $MnCl_2$ (5 mM). Reactions were initiated by addition of 3D^{pol} and incubated at 30 °C; reactions were quenched at the indicated times by addition of EDTA to a final concentration of 50 mM. Products were resolved by electrophoresis on a denaturing 20% polyacrylamide gel. *F*, kinetics of primer extension in the reaction described in *E* were determined by quantitating product by using the ImageQuant software.

of the value measured for incorporation of the correct rNTP. Incorrect rNTPs were utilized better than incorrect dNTPs, and ddNTPs were not utilized at all. Again, as discussed above, the $n + 1$ products observed in *lanes 9–11* of Fig. 8*B* must result from rNTP contamination of the ddNTP stocks. In the presence of Mn^{2+}, incorrect rNTPs were utilized efficiently. 53, 59, or 68% of primers were extended by using ATP (Fig. 8*C*, *lane 15*), CTP (Fig. 8*C*, *lane 16*), or GTP (Fig. 8*C*, *lane 17*), respectively, as the incorrect rNTP. In most instances, primers could not be extended to the end of template. The most significant accumulation of products was in the $n + 1$ to $n + 3$ range. Whereas utilization of dGTP was increased in the presence of Mn^{2+} (21% of primers extended), utilization of the other two incorrect dNTPs was similar to that observed in the presence of Mg^{2+}. The use of Mn^{2+} had very little effect on utilization of incorrect ddNTPs.

Finally, in some instances, an apparent activation of primer cleavage was observed. This increase in primer cleavage was apparent in the presence of Mg^{2+} (*lanes 6*, *9*, and *10* of Fig. 8*B*) and was stimulated by using Mn^{2+} (*lanes 15*, *19*, *20*, *21*, *23*, *24*, and *25* of Fig. 8*C*). Primer cleavage was not due to ribonuclease contamination of our 3D^{pol} preparations as cleavage was not observed in all reactions. Moreover, in most cases, ribonuclease activity does not require a divalent cation, thus an activity difference in the presence of Mg^{2+} relative to Mn^{2+} would not be expected (31). Interestingly, primer cleavage occurred primarily after misincorporation of nucleotides. Primer cleavage was not evident in reactions incorporating correct ribonucleotides (*lane 18*, Fig. 8*C*), deoxynucleotides (*lane 22*, Fig. 8*C*), or dideoxynucleotides (*lane 26*, Fig. 8*C*) Additional studies will be necessary to determine the molecular basis for this observation.

DISCUSSION

We have performed a comprehensive, quantitative evaluation of the divalent cation specificity of poliovirus RNA-dependent RNA polymerase, 3D^{pol}. The primary, universal effect of Mn^{2+} on 3D^{pol} was a substantial (20–30-fold) reduction in the K_M value of the enzyme for primer/template (Table III). 3D^{pol} activity was stimulated by an additional 20-fold over that expected based solely on the reduction in K_M value for primer/template when dG_{15}/rC_{30} was analyzed in the presence of Mn^{2+} (Table III). This additional increase in activity was not due to changes in the K_M value of 3D^{pol} for GTP as this value was not affected significantly by using Mn^{2+} instead of Mg^{2+} (Table III). Therefore, we concluded that by using Mn^{2+} the number of productive 3D^{pol}-dG_{15}/rC_{30} complexes formed was increased by 20-fold relative to the number formed by using Mg^{2+}.

The ability of nucleic acid polymerases to utilize transition metals, especially Mn^{2+}, as the divalent cation cofactor instead of Mg^{2+} is well established (33–37). The primary effect of Mn^{2+} relative to Mg^{2+} is that nucleotide specificity is relaxed, that is nucleotides with the inappropriate sugar or base can be incorporated more efficiently (35, 36). The classic explanation for the observed relaxation in nucleotide specificity in the presence of Mn^{2+} is that fewer geometrical constraints exist with this divalent cation for coordination of the nucleotide phosphates and active site ligands, which is a prerequisite to phosphoryl transfer (36). In fact, even for 3D^{pol}, it has been shown by Morrow and colleagues (38) that the use of transition metals as divalent cation cofactor for this enzyme can overcome, to some extent, effects of mutations at positions of the enzyme that alter the position or identity of the active site residues that are involved in metal coordination. Also, it has been noted that Mn^{2+} is capable of relaxing template specificity (39). In this regard, it worth noting that template specificity of 3D^{pol} was also relaxed by using Mn^{2+}; a DNA template supported RNA synthesis in the presence of this cofactor (Table II).

In this study, we observed a dramatic reduction in the K_M value for primer/template by employing Mn^{2+} as the divalent cation cofactor instead of Mg^{2+}. To date, similar observations have not been made for any other nucleic acid polymerase. However, the ability of Mg^{2+} to increase formation of productive polymerase-nucleic acid complexes has been noted previously by Modrich and colleagues (40). It has been shown that

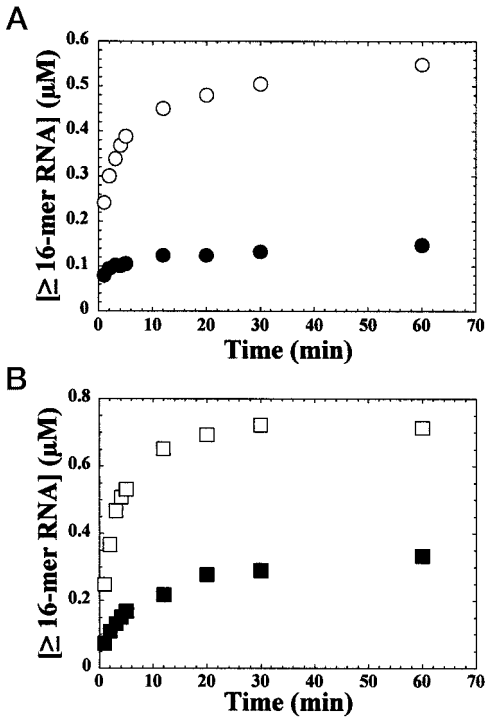

FIG. 5. **Comparison of the kinetics of primer extension using Mg^{2+} or Mn^{2+} as the divalent cation.** *A*, reactions contained 3D^{pol} (5 μM), end-labeled primer/template II (1 μM), ATP (500 μM), and either $MgCl_2$ (●) or $MnCl_2$ (○) (5 mM). Reactions were initiated by addition of 3D^{pol} and incubated at 30 °C; reactions were quenched at the indicated times by addition of EDTA to a final concentration of 50 mM. Products were resolved by electrophoresis on a denaturing 20% polyacrylamide gel, visualized by using a PhosphorImager and quantitated by using the ImageQuant software. *B*, reactions contained 3D^{pol} (5 μM), end-labeled primer/template II (1 μM), NTPs (500 μM), and either $MgCl_2$ (■) or $MnCl_2$ (□) (5 mM). Reactions were initiated by addition of 3D^{pol} and incubated at 30 °C; reactions were quenched at the indicated times by addition of EDTA to a final concentration of 50 mM. Products were resolved by electrophoresis on a denaturing 20% polyacrylamide gel, visualized by using a PhosphorImager and quantitated by using the ImageQuant software.

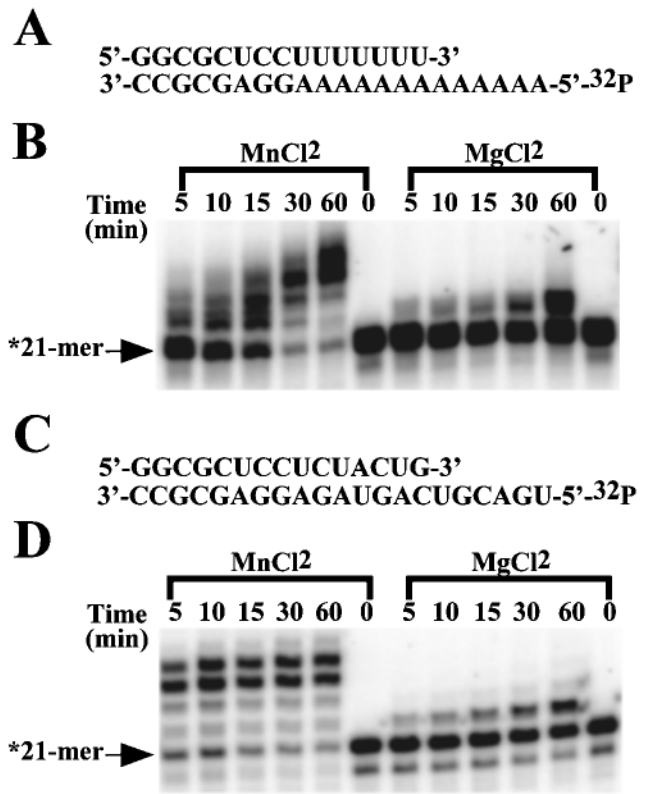

FIG. 6. **Addition of nontemplated nucleotides by 3D^{pol}.** *A*, 15/21-mer primer/template I employed in the experiment described in *B* was 5′-end-labeled on the template strand. *B*, reactions contained 3D^{pol} (5 μM), primer/template I (1 μM), NTPs (500 μM), and either $MnCl_2$ or $MgCl_2$ (5 mM). Reactions were initiated by addition of 3D^{pol} and incubated at 30 °C; reactions were quenched at the indicated times by addition of EDTA to a final concentration of 50 mM. Products were resolved by electrophoresis on a denaturing 20% polyacrylamide gel. *C*, 15/21-mer primer/template II employed in the experiment described in *D* was 5′-end-labeled on the template strand. *D*, reactions contained 3D^{pol} (5 μM), primer/template II (1 μM), NTPs (500 μM), and either $MnCl_2$ or $MgCl_2$ (5 mM). Reactions were initiated by addition of 3D^{pol} and incubated at 30 °C; reactions were quenched at the indicated times by addition of EDTA to a final concentration of 50 mM. Products were resolved by electrophoresis on a denaturing 20% polyacrylamide gel.

transition metals, such as Mn^{2+}, bind much more tightly to the phosphodiester backbone of nucleic acid than Mg^{2+} (41). Therefore, it is plausible that stability and/or concentration of primer/template duplex is increased due to the enhanced charge neutralization of the phosphodiester backbone in the presence of Mn^{2+}. If more primer/template duplex exists at lower concentrations in the presence of Mn^{2+} than in the presence of Mg^{2+}, then an apparent reduction in the K_M value for primer/template would be observed as this is the competent form of the substrate.

Alternatively, it is possible that 3D^{pol} has not evolved to bind to a charged template, that is the enzyme is incapable of effectively neutralizing the phosphodiester backbone. The strong binding of Mn^{2+} to the phosphodiester backbone would overcome this problem thereby increasing the affinity of 3D^{pol} for primer/template, in addition to possibly increasing the number of complexes that form. If this hypothesis is correct, then a mechanism for neutralization of the biological templates might exist. The virus-encoded 3AB protein may fulfill such a role because it has nonspecific RNA binding activity (42) and can increase the use of homo- and heteropolymeric primer/templates (43, 44). Similar scenarios have been well established for negative-strand RNA viruses such as Sendai virus (45).

We reported previously that 3D^{pol} is capable of primer-independent RNA synthesis when poly(rC) is employed as template (23). In this study, we demonstrated that primer-independent RNA synthesis resulted from initiation *de novo* and was also stimulated by using Mn^{2+} as the divalent cation cofactor. Overall, the reaction sequence employed by 3D^{pol} in catalyzing RNA synthesis *de novo* is quite similar to that observed for the same type of reaction catalyzed by replicases for RNA viruses such as Qβ (46) and brome mosaic virus (47). It is currently unclear whether RNA synthesis *de novo* catalyzed by 3D^{pol} has any biological significance. However, the ability of a polymerase that clearly uses a protein primer *in vivo* to support RNA synthesis *de novo* has significant implications on the conclusions that should be drawn when similar observations are made with polymerases from RNA virus systems which lack significant biological characterization. For example, a recent report on the RdRP from bovine viral diarrhea virus showed that this enzyme is capable of initiating RNA synthesis *de novo* (48). However, in the absence of data characterizing the 5′-end of viral RNA, it may be premature to completely rule out the possibility of primed synthesis in the mechanism of initiation of pesti- and hepacivirus genome replication.

The kinetics of primer extension were biphasic with both heteropolymeric primer/template substrates employed (Fig. 4, *C* and *F*). We anticipated that the reaction would be monophasic with the kinetics of formation of extended primers being described best by a single exponential. This assumption was based on the fact that the K_M values measured for dT_{15}/rA_{30}

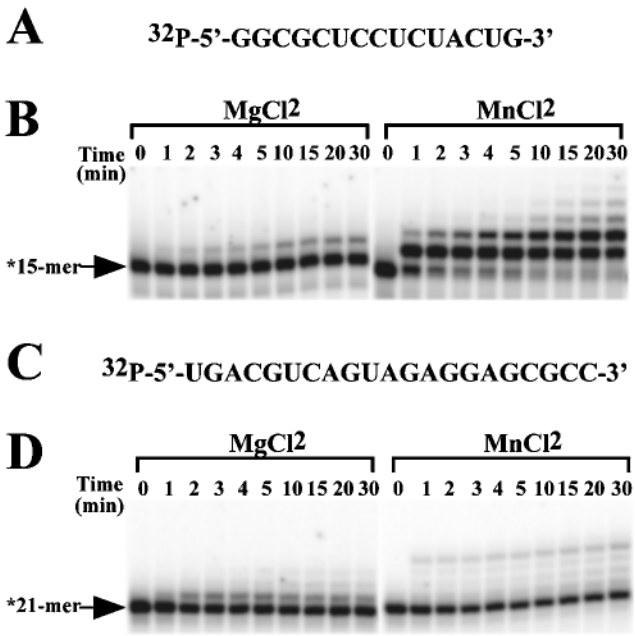

FIG. 7. **Terminal transferase activity by 3D^{pol}.** *A*, RNA oligonucleotide employed in the experiment described in *B* was 5′-end-labeled. *B*, reactions contained 3D^{pol} (5 μM), RNA (1 μM), ATP (500 μM), and either $MnCl_2$ or $MgCl_2$ (5 mM). Reactions were initiated by addition of 3D^{pol} and incubated at 30 °C; reactions were quenched at the indicated times by addition of EDTA to a final concentration of 50 mM. Products were resolved by electrophoresis on a denaturing 20% polyacrylamide gel. *C*, RNA oligonucleotide employed in the experiment described in *D* was 5′-end-labeled. *D*, reactions contained 3D^{pol} (5 μM), RNA (1 μM), ATP (500 μM), and either $MnCl_2$ or $MgCl_2$ (5 mM). Reactions were initiated by addition of 3D^{pol} and incubated at 30 °C; reactions were quenched at the indicated times by addition of EDTA to a final concentration of 50 mM. Products were resolved by electrophoresis on a denaturing 20% polyacrylamide gel.

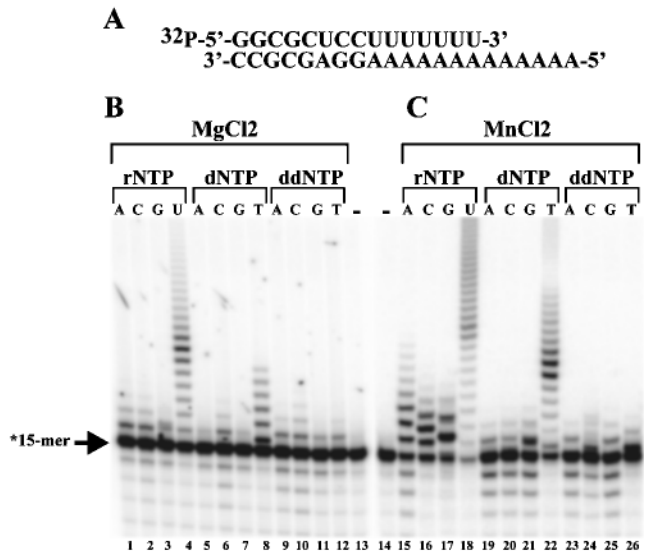

FIG. 8. **Nucleotide selection by 3D^{pol} in $MnCl_2$ and $MgCl_2$.** *A*, 15/21-mer primer/template I employed in this experiment. *B*, reactions contained 3D^{pol} (5 μM), primer/template I (1 μM), $MgCl_2$ (5 mM), and the indicated NTP or analog (500 μM). Reactions were initiated by addition of 3D^{pol} and incubated at 30 °C for 10 min. Products were resolved by electrophoresis on a denaturing 20% polyacrylamide gel. *C*, reactions contained 3D^{pol} (5 μM), primer/template I (1 μM), $MnCl_2$ (5 mM), and the indicated NTP or analog (500 μM). Reactions were initiated by addition of 3D^{pol} and incubated at 30 °C for 10 min. Products were resolved by electrophoresis on a denaturing 20% polyacrylamide gel.

and dG_{15}/rC_{30} in the presence of Mn^{2+} were in the 1 μM range, and a 3D^{pol} concentration of 5 μM was employed in this reaction, thus approximately 90% of the primer/template should be bound to enzyme.

One possible explanation for biphasic kinetics given the aforementioned assumptions was that two different 3D^{pol}-primer/template complexes formed. Whereas one complex would be competent for primer extension (first, fast phase), the other would be unproductive requiring some type of rearrangement of the initial enzyme-primer/template complex or enzyme dissociation from primer/template prior to formation of a complex that was competent for primer extension (second, slow phase). By employing a template-labeled primer/template, it was apparent that the enzyme was capable of binding to primer/template in both orientations and adding nucleotides to the blunt-end of the duplex (Fig. 6). That the addition was not terminal transferase activity was ruled out by qualitative and quantitative comparison of the single-stranded RNA primer or template (Fig. 7). Therefore, the "lost" fraction was found, and the slow phase, most likely, reflected dissociation of the enzyme from the unproductive conformation to bind to primer/template in the productive conformation.

Partitioning of the enzyme between the productive and unproductive conformations was not equal and differed for the two primer/template substrates employed in this study. Both substrates are identical in length of primer, template, and duplex region and only differ in three readily apparent ways. First, the sequence around the primer/template junction and template overhang are different. Second, there is a subtle (10 °C) difference in the calculated T_M values for the two primer/templates. Third, by using primer/template I and UTP, the enzyme can extend to the end of template, whereas by using primer/template II and ATP, extension to the end of template is not efficient as it requires misincorporation. This third possibility was ruled out as being a significant factor by showing that partitioning of primer/template II was not affected when reactions were performed in the presence of all four NTPs (Fig. 5). Given the two remaining possibilities, a sequence dependence for binding seems most likely. Additional experiments will be required to clarify this issue.

However, to gain insight into the nucleotide specificity and fidelity of 3D^{pol}, we performed a series of primer-extension experiments in which the utilization of correct and incorrect rNTPs, dNTPs, and ddNTPs was evaluated. Incorporation of dTMP was more efficient than incorporation of any of the incorrect rNMPs (*cf. lane 22* and *lanes 15*, *16*, and *17* of Fig. 8*C*). This result suggests that appropriate base pairing is more important for nucleotide incorporation than the presence of a 2′-OH, and the structural conformation of the duplex region of the nascent chain is important for processive synthesis, perhaps translocation. That the 2′-OH is recognized to some extent by 3D^{pol} was evident by evaluating misincorporation in the presence of Mn^{2+}. Whereas all three incorrect rNTPs could be utilized by 3D^{pol}, only one incorrect dNTP was utilized. However, this observation may result from conformational differences between ribose and deoxyribose other than the difference at the C2′ position. Thus, 3D^{pol} appears to utilize a two-step process for nucleotide selection. In the first step, the ability of the nucleotide to pair with the template is recognized; in the second step, the composition of the sugar is recognized. The use of Mn^{2+} permits this second step of nucleotide selection to be bypassed more easily. Consecutive cycles of misincorporation become increasingly more difficult as primer extension beyond $n + 2$ or $n + 3$ was rare (see *lanes 15–17* of Fig. 8*C*). Again, these data support the notion that the structural conformation and/or integrity of the duplex region of nascent chain is important for processive synthesis.

Finally, we noted that cleavage of the primer occurs in reac-

tions incorporating incorrect rNMPs and dNMPs. Primer cleavage occurred in the presence of Mg^{2+} and Mn^{2+} but was most striking in the presence of Mn^{2+}, because of the increased levels of misincorporation observed by using this cofactor. Primer cleavage may result from pyrophosphorolysis. If an appropriately base-paired duplex is a prerequisite to efficient translocation and PP_i release requires translocation (49), then it is conceivable that after misincorporation PP_i may have sufficient time to attack the misaligned duplex. However, our results would also suggest that PP_i is capable of attacking phosphodiester bonds other than the ultimate bond. Of course, this reaction could provide a mechanism for error correction. Studies are in progress to characterize this reaction more completely.

Acknowledgments—We thank Aniko Paul and Kevin Raney for critical evaluation of the manuscript.

REFERENCES

1. Houghton, M. (1996) in *Fields Virology* (Fields, B. N., Knipe, D. M., and Howley, P. M., eds) Vol. 1, pp. 1035–1058, Lippincott-Raven Publishers, Philadelphia, PA
2. Buck, K. W. (1996) *Adv. Virus Res.* **47,** 159–251
3. Ishihama, A., and Barbier, P. (1994) *Arch. Virol.* **134,** 235–258
4. Plotch, S. J., Palant, O., and Gluzman, Y. (1989) *J. Virol.* **63,** 216–225
5. Neufeld, K. L., Richards, O. C., and Ehrenfeld, E. (1991) *J. Biol. Chem.* **266,** 24212–24219
6. Behrens, S.-E., Tomei, L., and De Francesco, R. (1996) *EMBO J.* **15,** 12–22
7. Lohmann, V., Körner, F., Herian, U., and Bartenschlager, R. (1997) *J. Virol.* **71,** 8416–8428
8. Vázquez, A. L., Martín, J. M., Casais, R., Boga, J. A., and Parra, F. (1998) *J. Virol.* **72,** 2999–3004
9. Rueckert, R. R. (1996) in *Fields Virology* (Fields, B. N., Knipe, D. M., and Howley, P. M., eds) Vol. 1, pp. 609–654, Lippincott-Raven Publishers, Philadelphia, PA
10. Xiang, W., Paul, A. V., and Wimmer, E. (1997) *Semin. Virol.* **8,** 256–273
11. Andino, R., Rieckhof, G. E., Achacoso, P. L., and Baltimore, D. (1993) *EMBO J.* **12,** 3587–3598
12. Xiang, W., Cuconati, A., Hope, D., Kirkegaard, K., and Wimmer, E. (1998) *J. Virol.* **72,** 6732–6741
13. Gamarnik, A. V., and Andino, R. (1996) *EMBO J.* **15,** 5988–5998
14. Barton, D. J., Black, E. P., and Flanegan, J. B. (1995) *J. Virol.* **69,** 5516–5527
15. Barton, D. J., and Flanegan, J. B. (1997) *J. Virol.* **71,** 8482–8489
16. Paul, A. V., van Boom, J. H., Filippov, D., and Wimmer, E. (1998) *Nature* **393,** 280–284
17. Neufeld, K. L., Galarza, J. M., Richards, O. C., Summers, D. F, and Ehrenfeld, E. (1994) *J. Virol.* **68,** 5811–5818
18. Cho, M. W., Richards, O. C., Dmitrieva, T. M., Agol, V., and Ehrenfeld, E. (1993) *J. Virol.* **67,** 3010–3018
19. Hansen, J. L., Long, A. M., and Schultz, S. C. (1997) *Structure* **5,** 1109–1122
20. Beckman, M. T. L., and Kirkegaard, K. (1998) *J. Biol. Chem.* **273,** 6724–6730
21. Pata, J. D., Schultz, S. C., and Kirkegaard, K. (1995) *RNA* (*N. Y.*) **1,** 466–477
22. Diamond, S. E., and Kirkegaard, K. (1994) *J. Virol.* **68,** 863–876
23. Arnold, J. J., and Cameron, C. E. (1999) *J. Biol. Chem.* **274,** 2706–2716
24. Gohara, D. W., Ha, C. S., Ghosh, S. K. B., Arnold, J. J., Wisniewski, T. J., and Cameron, C. E. (1999) *Protein Expression Purif.* **17,** 128–138
25. Carroll, S. S., Benseler, F., and Olsen, D. B. (1996) *Methods Enzymol.* **275,** 365–382
26. Arnold, J. J., Ghosh, S. K. B., Bevilacqua, P. C., and Cameron, C. E. (1999) *BioTechniques* **27,** 450–456
27. Binz, P.-A., Wilkins, M. R., Gasteiger, E., Bairoch, A., Appel, R. D., and Hochstrasser, D. F. (1999) in *Internet Resources for Protein Identification and Characterization: Microcharacterization of Proteins* (Kellner, R., Lottspeich, F., and Meyer, H. E., eds) pp. 277–300, Wiley-VCH, New York
28. Gill, S. C., and von Hippel, P. H. (1989) *Anal. Biochem.* **182,** 319–326
29. Serra, M. J., and Turner, D. H. (1995) *Methods Enzymol.* **259,** 242–261
30. Peliska, J. A., and Benkovic, S. J. (1992) *Science* **258,** 1112–1118
31. Thompson, J. E., and Raines, R. T. (1994) *J. Am. Chem. Soc.* **116,** 5467–5468
32. Deleted in proofs
33. Grabbara, S., and Peliska, J. A. (1996) *Methods Enzymol.* **275,** 276–310
34. Cirino, N. M., Cameron, C. E., Smith, J. S., Rausch, J. W., Roth, M. J., Benkovic, S. J., and Le Grice, S. F. J. (1995) *Biochemistry* **34,** 9936–9943
35. Tabor, S., and Richardson, C. C. (1989) *Proc. Natl. Acad. Sci. U. S. A.* **86,** 4076–4080
36. Huang, Y., Beaudry, A., McSwiggen, J., and Sousa, R. (1997) *Biochemistry* **36,** 13718–13728
37. Brooks, R. R., and Anderson, J. A. (1978) *Biochem. J.* **171,** 725–732
38. Jablonski, S. A., and Morrow, C. D. (1995) *J. Virol.* **69,** 1532–1539
39. Palmenberg, A., and Kaesberg, P. (1974) *Proc. Natl. Acad. Sci. U. S. A.* **71,** 1371–1375
40. Hsieh, J.-C., Zinnen, S., and Modrich, P. (1993) *J. Biol. Chem.* **268,** 24607–24613
41. Knoll, D. A., Fried, M. G., and Bloomfield, V. A. (19??) in *Structure and Expression, Volume 2: DNA and Its Drug Complexes* (Sarma, R. H., and Sarma, M. H., eds) pp. 123–145, Adenine Press, New York
42. Xiang, W., Cuconati, A., Paul, A. V., Cao, X., and Wimmer, E. (1995) *RNA* (*N. Y.*) **1,** 892–904
43. Paul, A. V., Cao, X., Harris, K. S., Lama, J., and Wimmer, E. (1994*) J. Biol. Chem.* **269,** 29173–29181
44. Richards, O. C., and Ehrenfeld, E. (1998) *J. Biol. Chem.* **273,** 12832–12840
45. Lamb, R. A., and Kolakofsky, D. (1996) in *Fields Virology* (Fields, B. N., Knipe, D. M., and Howley, P. M., eds) Vol. 1, pp. 1177–1204, Lippincott-Raven Publishers, Philadelphia, PA
46. Spiegelman, S., Pace, N. R., Mills, D. R., Levisohn, R., Eikhom, T. S., Taylor, M. M., Peterson, R. L., and Bishop, D. H. L. (1968) *Cold Spring Harbor Symp. Quant. Biol.* **33,** 101–124
47. Adkins, S., Stawicki, S. S., Faurote, G., Siegel, R. W., and Kao, C. C. (1998) *RNA* (*N. Y.*) **4,** 455–470
48. Kao, C. C., Del Vecchio, A. M., and Zhong, W. (1999) *Virology* **253,** 1–7
49. Kati, W. M., Johnson, K. A., Jerva, L. F., and Anderson, K. S. (1992) *J. Biol. Chem.* **267,** 25988–25997

Poliovirus RNA-dependent RNA Polymerase ($3D^{pol}$): DIVALENT CATION MODULATION OF PRIMER, TEMPLATE, AND NUCLEOTIDE SELECTION

Jamie J. Arnold, Saikat Kumar B. Ghosh and Craig E. Cameron

J. Biol. Chem. 1999, 274:37060-37069.
doi: 10.1074/jbc.274.52.37060
